Effects of strain on the band structure of group-III nitrides

Qimin Yan,[1,2] Patrick Rinke,[3] Anderson Janotti,[1] Matthias Scheffler,[1,3] and Chris G. Van de Walle[1]

[1]*Materials Department, University of California, Santa Barbara, California 93106-5050, USA*

[2]*Molecular Foundry, Lawrence Berkeley National Laboratory, Berkeley, California 94720, USA*

[3]*Fritz-Haber-Institut der Max-Planck-Gesellschaft, Faradayweg 4–6, D-14195 Berlin, Germany*

We present a systematic study of strain effects on the electronic band structure of the group-III-nitrides (AlN, GaN and InN) in the wurtzite phase. The calculations are based on density functional theory with band-gap-corrected approaches including the Heyd-Scuseria-Ernzerhof hybrid functional (HSE) and quasiparticle G_0W_0 methods. We study strain effects under realistic strain conditions, hydrostatic pressure, and biaxial stress. The strain-induced modification of the band structures is found to be nonlinear; transition energies and crystal-field splittings show a strong nonlinear behavior under biaxial stress. For the linear regime around the experimental lattice parameters, we present a complete set of deformation potentials (a_{cz}, a_{ct}, D_1, D_2, D_3, D_4, D_5, D_6) that allows us to predict the band positions of group-III nitrides and their alloys (InGaN and AlGaN) under realistic strain conditions. The benchmarking G_0W_0 results for GaN agree well with the HSE data and indicate that HSE provides an appropriate description for the band structures of nitrides. We present a systematic study of strain effects on the electronic band structure of the group-III nitrides (AlN, GaN, and InN). We quantify the nonlinearity of strain effects by introducing a set of bowing parameters. We apply the calculated deformation potentials to the prediction of strain effects on transition energies and valence-band structures of InGaN alloys and quantum wells (QWs) grown on GaN, in various orientations (including c-plane, m-plane, and semipolar). The calculated band gap bowing parameters, including the strain effect for c-plane InGaN, agree well with the results obtained by hybrid functional alloy calculations. For semipolar InGaN QWs grown in $(20\bar{2}1)$, $(30\bar{3}1)$, and $(30\bar{3}\bar{1})$ orientations, our calculated deformation potentials have provided results for polarization ratios in good agreement with the experimental observations, providing further confidence in the accuracy of our values.

I. INTRODUCTION

The group-III nitride semiconductors AlN, GaN, InN, and their alloys are already extensively used in light-emitting diodes [1] and laser diodes [2] from the visible spectrum to the deep ultraviolet (UV). The electronic structure of these wide-band-gap semiconductors also enables high-power and high-frequency devices [3]. However, the application of nitride semiconductors is currently still limited by several factors. For solid-state lighting, one of the most serious limitations is the droop problem, which is believed to be related to the Auger recombination process [4–6]. In addition, in traditional c-plane (polar) quantum wells (QWs), the electron and hole wave functions are separated by polarization fields, which lowers the radiative recombination rate. To overcome this problem, and to allow wider QWs that would also mitigate Auger losses, semipolar and nonpolar InGaN/GaN QWs have been proposed, where the polarization fields can be greatly reduced or even eliminated [7]. Several experimental groups have reported nitride-based light-emitting devices grown on these nonpolar and semipolar planes [8–12].

One effect of forming an interface between dissimilar nitride materials is the development of strain. The active regions in nitride-based light-emitting devices consist of heterostructures such as InGaN/GaN (in light-emitting devices) or AlGaN/GaN (in power electronic devices) multiple-quantum-well (MQW) structures. Due to the large lattice mismatch (2.5% between AlN and GaN and 11.0% between InN and GaN), strain is present in alloy layers that are pseudomorphically grown on thick GaN layers or substrates. Strain affects the device properties in several ways: (a) It changes the absolute positions of the valence-band maximum (VBM) and the conduction-band minimum (CBM), and hence modifies the QW depth and the confinement of electrons and holes in the active region. (b) It induces piezoelectric polarization in InGaN or AlGaN QWs [7,13,14], thus lowering the electron-hole overlap and hence the radiative recombination rate. (c) It may also modify the effective masses of carriers and the density of states [15,16]. (d) In polar (c-plane) QWs, the in-plane strain is isotropic [17–19]. In nonpolar and semipolar QWs, on the other hand, the biaxial stress induces anisotropic strain, which drastically modifies the subband structures and wave-function character [20–22] and induces polarized light emission [11,12,14].

The effects of strain on the band structures of semiconductors can, to first order, be described by deformation potentials. These are the linear coefficients in the response of the band structure to a strain perturbation. The applicability of such a description has been demonstrated in measurements of the optical transition energies for GaN epilayers with residual strain [23–25]. To quantify the strain effects for InGaN or AlGaN alloys, accurate deformation potential parameters for all three nitrides are needed.

So far, most of the experimental data on deformation potentials of GaN [25–27,40] and InN [28] have been obtained by a combination of x-ray and optical measurements from the change of optical transition energies under the biaxial stress induced by the c-plane substrate. However, the accurate determination of deformation potentials by this experimental approach is difficult. Indeed, as shown in Table I, the experimental deformation potential data of GaN scatter over a very large range. One of the main problems is that the uniaxial and

TABLE I. Literature results for deformation potentials (eV) of wurtzite GaN.

Method	$a_{cz} - D_1$	$a_{ct} - D_2$	D_3	D_4	D_5	D_6
Calc.[a]			2.99	−1.50	−2.04	
Calc.[b]	−4.78	−6.18	1.40	−0.70		
Calc.[c]	−3.10	−11.2	8.20	−4.10	−4.70	
Calc.[d]			5.80	−3.25	−2.85	
Calc.[e]	−6.11	−9.62	5.76	−3.04		
Calc.[f]	−9.47	−7.17	6.26	−3.29		
Calc.[g]	−6.02	−8.98	5.45	−2.97	−2.87	−3.95
Expt.[h]			8.82	−4.41		
Expt.[i]	−6.50	−11.80	5.30	−2.70		
Expt.[j]			6.80	−3.40	−3.30	
Expt.[k]	−5.32	−10.23	4.91	−2.45		
Expt.[l]					−3.60	
Expt.[m]	−9.60	−8.20	1.90	−1.00		
Expt.[n]	−6.50	−11.20	4.90	−5.00	−2.80	−3.10

[a]Reference [32].
[b]Reference [33].
[c]Reference [34].
[d]Reference [35].
[e]Reference [36].
[f]Reference [37].
[g]References [38,39].
[h]Reference [27].
[i]Reference [26].
[j]Reference [40].
[k]Reference [25].
[l]Reference [41].
[m]Reference [42].
[n]Reference [30].

biaxial strain components cannot be applied separately, and the measurement only provides results for a combination of several deformation potentials. The quasicubic approximation [29] is then needed to extract the deformation potentials from these data—and as we will discuss in Sec. III D, this approximation is not valid in the wurtzite nitrides. Uncertainties in the results of the studies that use this approximation are thus to be expected [25–27,40]. Another complication is that the determination of the out-of-plane strain component depends on the numerical values of the elastic stiffness constants. The values of these constants also exhibit a lot of scatter.

A fairly unique approach was reported in Ref. [42], where uniaxial strain along the c axis of GaN was applied by shock compression. However, the $a_{cz} - D_1$ value obtained using this approach is larger in magnitude than any of the other results, while the D_3 and D_4 values are much smaller in magnitude. This might possibly be due to the biaxial strain components not being exactly zero during the shock compression.

The most reliable experimental approach may be to carry out optical measurements under various types of static uniaxial stress. Such techniques have recently been used to obtain the deformation potentials of GaN [30] and AlN [31]. The advantage of this approach is that various strained environments can be introduced in the system of interest, and therefore deformation potentials are obtained without needing to rely on the quasicubic approximation. Overall, as shown in Table I,

the experimental results measured using this approach show better agreement with the most recent theoretical predictions.

Theoretical values are also available for GaN, but they similarly are spread over a large range, as shown in Table I. The large deviations in the band-gap-related deformation potentials ($a_{cz} - D_1, a_{ct} - D_2$) can be attributed to the band-gap problem of density functional theory (DFT) in the local density approximation (LDA) or the generalized gradient approximation (GGA). Although DFT with present-day exchange-correlation functionals performs exceptionally well in predicting the ground-state properties of materials, it was not intended to describe properties that involve electronic excitations. One of the most serious drawbacks of traditional DFT functionals, in particular LDA and GGA, is that the band gaps of Kohn-Sham band structures are severely underestimated (typically by 50%). For InN, this would be an even worse problem, since LDA or GGA calculations give a negative band gap and hence incorrect interactions between bands, prohibiting a determination of deformation potentials of InN with those techniques. Recently, several schemes have been developed to address this problem, including the incorporation of exact exchange in hybrid functionals and applying many-body perturbation theory on top of traditional DFT calculations. Deformation potentials calculated with these advanced methods show better agreement with experiment [38].

In addition, it has been shown that the relaxation of the internal displacement parameter u is critical in determining the crystal-field splitting and the related deformation potentials (D_3 and D_4) [35]. Some earlier work that did not include this internal relaxation is therefore not reliable [33]. Furthermore, due to the sensitivity of the deformation potentials to u, the results may not be accurate unless convergence is explicitly verified. Finally, as we will demonstrate in Sec. III B, the equilibrium lattice parameters around which the linear expansion is constructed also has a large effect on the deformation potentials, due to the pronounced nonlinear dependence of some of the transition energies on strain. Different theoretical approaches may yield different equilibrium lattice parameters.

In the present work, all of these shortcomings of previous theoretical approaches have been addressed. We study the strain effects on the band structure of wurtzite AlN, GaN, and InN using band-gap-corrected first-principles approaches including hybrid functionals [43] and the quasiparticle G_0W_0 method [44]. We show that the strain-induced modification of the band structures is nonlinear, and we quantify this nonlinearity by introducing a set of bowing parameters. By applying different strains to wurtzite nitrides, we obtain a complete set of deformation potentials for the linear regime around the experimental lattice parameters. These results will be reported in Sec. III.

In Sec. IV, we then use the semiempirical **k·p** method to explore the strain effects in InGaN alloys by applying our consistent set of deformation potentials. This allows us to predict the band-structure modifications due to strain in polar c-plane and nonpolar m-plane InGaN/GaN systems: (a) the effect of biaxial stress on band gaps of InGaN alloys grown on c-plane GaN substrates; (b) the relation between anisotropic in-c-plane biaxial strain on valence-band structures and the optical anisotropy of the light emitted from m-plane InGaN/GaN devices [45]; and (c) the role of strain in the

valence-band structure and polarization of semipolar InGaN alloys.

II. MODEL AND COMPUTATIONAL DETAILS

A. k·p perturbation approach

We employ the **k·p** perturbation approach of Bir and Pikus [29] to obtain the analytical solutions of strain-induced band-structure modifications in the vicinity of the Γ point. These solutions are then used to fit the first-principles band structures to extract the deformation-potential parameters. The strained Hamiltonian of the topmost three valence bands is given by the following 6×6 matrix:

$$
H = \begin{bmatrix}
F & 0 & -H^* & 0 & K^* & 0 \\
0 & G & \Delta & -H^* & 0 & K^* \\
-H & \Delta & \lambda & 0 & I^* & 0 \\
0 & -H & 0 & \lambda & \Delta & I^* \\
K & 0 & I & \Delta & G & 0 \\
0 & K & 0 & I & 0 & F
\end{bmatrix}, \quad (1)
$$

where

$$
\begin{aligned}
F &= \Delta_1 + \Delta_2 + \lambda + \theta, \\
G &= \Delta_1 - \Delta_2 + \lambda + \theta, \\
H &= i(A_6 k_z k_+ + A_7 k_+ + D_6 \varepsilon_{z+}), \\
I &= i(A_6 k_z k_+ - A_7 k_+ + D_6 \varepsilon_{z+}), \\
K &= A_5 k_+^2 + D_5 \varepsilon_+, \\
\Delta &= \sqrt{2}\Delta_2, \\
\lambda &= A_1 k_z^2 + A_2 k_\perp^2 + D_1 \varepsilon_{zz} + D_2(\varepsilon_{xx} + \varepsilon_{yy}), \\
\theta &= A_3 k_z^2 + A_4 k_\perp^2 + D_3 \varepsilon_{zz} + D_4(\varepsilon_{xx} + \varepsilon_{yy}), \\
\varepsilon_+ &= \varepsilon_{xx} - \varepsilon_{yy} + 2i\varepsilon_{xy}, \quad \varepsilon_{z+} = \varepsilon_{xz} + i\varepsilon_{yz}, \\
k_+ &= k_x + ik_y, \quad k_\perp^2 = k_x^2 + k_y^2.
\end{aligned}
$$

Here k_x, k_y, and k_z are the electron wave vectors along the x, y, and z directions. The x, y, and z directions are defined as the $[10\bar{1}0]$, $[1\bar{1}00]$, and $[0001]$ directions of the hexagonal lattice, respectively. ε_{xx}, ε_{yy}, and ε_{zz} are the strain components along the x, y, and z directions, respectively. ε_{xz} and ε_{yz} are shear-strain components in the xz and yz planes. Δ_1 is the crystal-field interaction and Δ_2 is the spin-orbit interaction. Note that the element H in this Hamiltonian is different in sign and by a factor i from that in the approach of Chuang and Chang [33]. However, these differences do not produce any observable physical effect; previous work has shown that the same band structure is obtained from both approaches [46]. We have also checked that such a difference in the Hamiltonian does not affect the dependence of the band energies at the Γ point on the strain components, which is used to extract the deformation potentials. Therefore, the Chuang-Chang [33] and Bir-Pikus [29] approaches are equivalent.

For an unstrained wurtzite system, the top three valence bands correspond to the heavy hole (HH), light hole (LH), and crystal-field split-off band (CH). The transition energies from the CBM to these three bands are denoted E_A, E_B, and E_C, respectively. Here we do not consider the spin-orbit interaction

($\Delta_2 = 0$), which is very small in the nitrides [47]. In this case, the HH and LH bands become doubly degenerate (Γ_6) in the absence of strain, and the CH band (Γ_1) is split off by the crystal-field splitting.

We first focus on those strain components that do not break the wurtzite symmetry, including biaxial strain in the c plane ($\varepsilon_{xx} = \varepsilon_{yy}$) and uniaxial strain along the c axis (ε_{zz}). Such strain perturbations to the 6×6 **k·p** Hamiltonian do not split HH and LH bands, although they induce an energy shift of the conduction and the three valence bands at the Γ point:

$$
\begin{aligned}
\Delta E_{\text{CB}} &= a_{\text{cz}}\varepsilon_{zz} + a_{\text{ct}}\varepsilon_\perp, \\
\Delta E_{\text{HH/LH}} &= (D_1 + D_3)\varepsilon_{zz} + (D_2 + D_4)\varepsilon_\perp, \\
\Delta E_{\text{CH}} &= D_1 \varepsilon_{zz} + D_2 \varepsilon_\perp, \quad (2)
\end{aligned}
$$

yielding the following transition energies:

$$
\begin{aligned}
E_{A/B} &= E_{A/B}(0) + (a_{\text{cz}} - D_1)\varepsilon_{zz} + (a_{\text{ct}} - D_2)\varepsilon_\perp \\
&\quad - (D_3 \varepsilon_{zz} + D_4 \varepsilon_\perp), \\
E_C &= E_C(0) + (a_{\text{cz}} - D_1)\varepsilon_{zz} + (a_{\text{ct}} - D_2)\varepsilon_\perp. \quad (3)
\end{aligned}
$$

Here $\varepsilon_\perp$ (defined as $\varepsilon_{xx} + \varepsilon_{yy}$) and ε_{zz} are the strain components in and out of the c plane. $E_{A/B}(0)$ and $E_C(0)$ are the corresponding transition energies at equilibrium lattice constants. From the slopes of the transition energies under biaxial strain in the c plane ($\varepsilon_{xx} = \varepsilon_{yy} \neq 0, \varepsilon_{zz} = 0$), we obtain the deformation potentials $a_{\text{ct}} - D_2$ and D_4, while $a_{\text{cz}} - D_1$ and D_3 can be obtained from the slope of transition energies under uniaxial strain along the c axis ($\varepsilon_{xx} = \varepsilon_{yy} = 0, \varepsilon_{zz} \neq 0$).

The strain components mentioned above preserve the symmetry of the wurtzite crystal. The hexagonal symmetry can be broken by anisotropic strain in the c plane, which is present in nonpolar and semipolar nitride alloys. For example, uniaxial strain in the c plane ($\varepsilon_{yy} = \varepsilon_{zz} = 0, \varepsilon_{xx} \neq 0$) changes the crystal symmetry from C_{6v} to C_{2v}. Without spin-orbit splitting, the original 6×6 Hamiltonian reduces to a 3×3 matrix. Anisotropic strain in the c plane lifts the degeneracy of the Γ_6 states and yields the three eigenenergies:

$$
\begin{aligned}
E_1 &= E_{A/B}(0) + (D_2 + D_4)\varepsilon_{xx} + D_5 \varepsilon_{xx}, \\
E_2 &= E_{A/B}(0) + (D_2 + D_4)\varepsilon_{xx} - D_5 \varepsilon_{xx}, \quad (4) \\
E_3 &= E_C(0) + D_2 \varepsilon_{xx}.
\end{aligned}
$$

Correspondingly, the three eigenstates are

$$
\begin{pmatrix} 1 \\ 1 \\ 0 \end{pmatrix}, \quad \begin{pmatrix} -1 \\ 1 \\ 0 \end{pmatrix}, \quad \begin{pmatrix} 0 \\ 0 \\ 1 \end{pmatrix}. \quad (5)
$$

The basis of the eigenvectors is

$$
\begin{aligned}
|1\rangle &= |X + iY\rangle, \\
|2\rangle &= |X - iY\rangle, \quad (6) \\
|3\rangle &= |Z\rangle,
\end{aligned}
$$

where the characters $X/Y/Z$ indicate that the corresponding wave function has $p_x/p_y/p_z$ character. The first eigenvector in Eq. (5) has p_x character, while the second eigenvector has p_y character. We obtain the magnitude of the deformation potential D_5 from the slope of the energy splitting between the
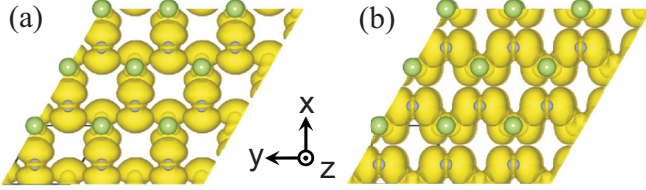
FIG. 1. (Color online) Partial charge density of (a) the highest and (b) the second highest valence band of wurtzite GaN under compressive uniaxial strain in the c plane.

top two valence bands under anisotropic strain:

$$\Delta E = |E_X - E_Y| = 2|D_5 \varepsilon_{xx}|. \tag{7}$$

To determine the sign of D_5, we need to explore the symmetry character of the valence bands. Figure 1 shows the partial charge density of the topmost two valence bands of wurtzite GaN under uniaxial compressive strain along the x direction. The highest valence state exhibits p_x character, while the second highest state exhibits p_y character. This implies that D_5 is negative in GaN, in agreement with experimental observations [40]. Based on the calculated partial charge densities of AlN and InN (not shown here), we find that the D_5 values in AlN and InN are also negative.

Another strain component that is present in semipolar nitride materials is shear strain (ε_{xz} and ε_{yz}). The corresponding deformation potential is D_6. By applying only the shear strain ε_{xz} in the wurtzite system, neglecting the spin-orbit interaction, the topmost three valence-band eigenenergies at the Γ point are

$$E_1 = \Delta_{\mathrm{cr}},$$

$$E_2 = \frac{\Delta_{\mathrm{cr}}}{2} + \frac{\sqrt{\Delta_{\mathrm{cr}}^2 + 8D_6^2 \varepsilon_{xz}^2}}{2}, \tag{8}$$

$$E_3 = \frac{\Delta_{\mathrm{cr}}}{2} - \frac{\sqrt{\Delta_{\mathrm{cr}}^2 + 8D_6^2 \varepsilon_{xz}^2}}{2}.$$

We obtain the valence-band structures of the shear-strained wurtzite GaN system from first-principles calculations. The energy separation between E_2 and E_3 is defined as $\Delta E_{23} = \sqrt{\Delta_{\mathrm{cr}}^2 + 8D_6^2 \varepsilon_{xz}^2}$. The energy of one of the doubly degenerate valence bands (E_1, with p_y character) stays constant, while the other one (E_2, with p_x character) goes up. Correspondingly, the crystal-field split-off band (E_3, with p_z character) goes down with the same magnitude.

Above, we have presented the definitions of all deformation potentials that are needed to describe the modification of the band structure with strain at the Γ point. To determine these deformation potentials from first-principles calculations, we apply different strain components in the wurtzite nitride systems and then fully relax the structure including the internal structural parameter u (which sensitively affects the magnitude of the crystal-field splitting). By fitting the analytical expressions for the $\mathbf{k}\cdot\mathbf{p}$ eigenenergies at the Γ point to the calculated band structures with different strain components, the deformation potentials are obtained.

B. First-principles calculations

The DFT calculations are carried out using the plane-wave projector augmented-wave (PAW) [48] method as implemented in the VASP code [49]. We use the Heyd-Scuseria-Ernzerhof (HSE) [43,50] hybrid functional to carry out the structural optimization as well as band-structure calculations, which gives band gaps and equilibrium lattice parameters in better agreement with experiment for nitrides than LDA and GGA, as shown in our previous work [38]. The screening parameter μ in HSE is fixed at a value of 0.2. With the default mixing parameter (25%), the obtained band gap of InN (0.68 eV) agrees pretty well with experiment(0.7 eV). For AlN and GaN, the mixing parameter α is modified (34% for AlN, 30% for GaN) to reproduce the experimental band gaps (6.13 eV for AlN, 3.48 eV for GaN). We treat the semicore d electrons of Ga and In as valence electrons (also in the G_0W_0 calculations). We use a plane-wave energy cutoff of 600 eV, which is necessary for the accurate determination of the internal displacement parameter u, and a $6 \times 6 \times 4\Gamma$-point centered k-point mesh. Our quasiparticle G_0W_0 calculations were based on exact exchange in the optimized effective potential approach (G_0W_0@OEPx) [44].

III. COMPUTATIONAL RESULTS

A. Equilibrium lattice parameters and band gaps

The lattice parameters of the wurtzite crystal structure for AlN, GaN, and InN are shown in Table II. LDA underestimates the equilibrium lattice parameters of AlN, GaN, and InN, while GGA overestimates these parameters compared with

TABLE II. Equilibrium lattice parameters (a and c) and band gaps (E_g) obtained with LDA, GGA, HSE (with different mixing parameter α), and the G_0W_0 quasiparticle approach. For the cases with modified mixing parameter α, the band gaps are obtained at experimental lattice parameters. The experimental lattice parameters at which the G_0W_0 band gaps are obtained are listed in the G_0W_0 rows. Experimental lattice parameters at $T = 300$ K are taken from Ref. [51], and band gaps at low temperature are taken from Refs. [52] and [53].

|	Method	a (Å)	c (Å)	u	E_g (eV)
AlN	LDA	3.092	4.950	0.3818	4.40
	GGA	3.127	5.021	0.3812	4.10
	HSE ($\alpha = 0.25$)	3.102	4.971	0.3819	5.64
	HSE ($\alpha = 0.34$)	3.096	4.957	0.3820	6.13
	G_0W_0	3.112	4.982	0.382	6.47
	Expt.	3.112	4.982	0.382	6.15
GaN	LDA	3.155	5.145	0.3764	2.12
	GGA	3.215	5.240	0.3766	1.74
	HSE ($\alpha = 0.25$)	3.182	5.173	0.3772	3.27
	HSE ($\alpha = 0.30$)	3.174	5.162	0.3773	3.48
	G_0W_0	3.190	5.189	0.377	3.24
	Expt.	3.190	5.189	0.377	3.51
InN	LDA	3.504	5.670	0.3784	<0
	GGA	3.573	5.762	0.3792	<0
	HSE ($\alpha = 0.25$)	3.548	5.751	0.3796	0.68
	G_0W_0	3.540	5.706	0.380	0.69
	Expt.	3.540	5.706	0.380	0.7
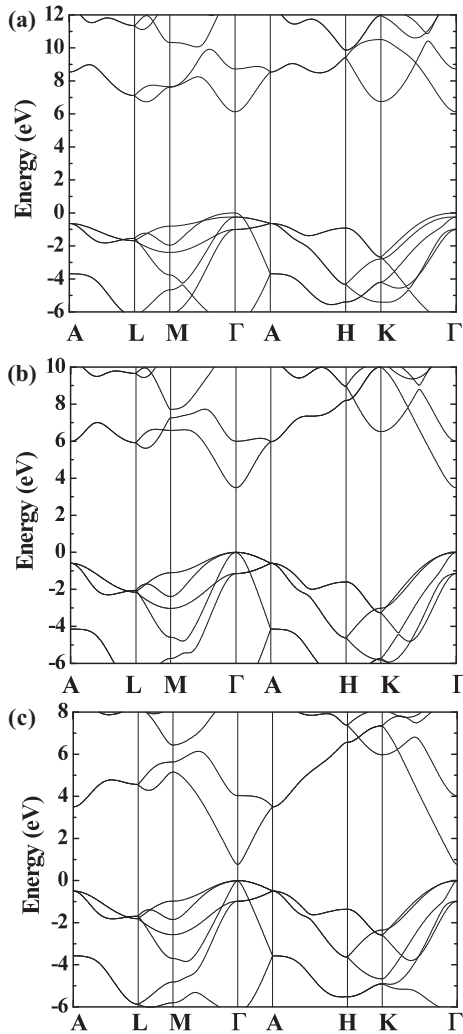
FIG. 2. Band structures of (a) AlN, (b) GaN, and (c) InN at the experimental lattice parameters, calculated using DFT and the HSE hybrid functional with mixing parameters α adjusted to reproduce the experimental band gap (see text).

experimental data. The deviations are on the order of 1%, which is typical of these functionals. The HSE results for structural properties with the default mixing parameter are typically closer to experiment. The HSE band structures obtained in Ref. [38] were obtained with the default mixing parameter $\alpha = 25\%$. Although better agreement with experiment compared with LDA or GGA was achieved, the calculated band gaps for the three nitrides were still smaller than experiment. Better agreement with experimental band gaps can be achieved by modifying the mixing parameter. The mixing parameters needed to reproduce the experimental band gaps of group-III nitrides at the experimental lattice parameters are 34% for AlN and 30% for GaN. As shown in Table II, the modified mixing parameter also provides good agreement with experiment for the structural properties.

The band structures of group-III nitride semiconductors AlN, GaN, and InN obtained with the hybrid functional approach with modified mixing parameters are shown in Fig. 2. These band structures show good agreement with results

obtained with the quasiparticle G_0W_0@OEPx method [51], which serves as a validation of the use of HSE as a reliable method to obtain accurate band structures.

B. Transition energies in GaN under realistic strain

Optical transitions from the lowest conduction band to the topmost three valence bands are dominant for optical emission processes in nitride materials. In GaN, these transitions have also been used as a characterization tool to evaluate the effects of strain on the electronic properties. In this section, we will analyze the strain dependence of these transition energies in c-plane GaN by computing the band structures of GaN for two types of realistic strain conditions: biaxial stress and hydrostatic pressure.

Wurtzite c-plane GaN thin films grown on sapphire or SiC experience biaxial stress induced by the substrate. Under such stress, the wurtzite system exhibits biaxial strain in the c plane accompanied by out-of-plane strain along the c axis:

$$\varepsilon_{zz} = -2\frac{C_{13}}{C_{33}}\varepsilon_{xx}, \quad \varepsilon_{xx} = \varepsilon_{yy} \neq 0. \tag{9}$$

Here we use the elastic constants C_{13} and C_{33} obtained by DFT calculations performed within the LDA [54] to determine the strain components and lattice parameters under biaxial stress.

Figure 3(a) shows the transition energies between the lowest conduction band and the topmost three valence bands (HH, LH, and CH) of GaN under biaxial stress in the c plane for the strain range $\pm 3\%$. Interestingly, the transitions between the CB and HH or LH bands show a strong nonlinear behavior. Such nonlinearity is also evident in the crystal-field splitting (Δ_{cr}) in Fig. 3(b), which can be described by a quadratic dependence as demonstrated by the fitted curve. This implies that the slope (which defines the deformation potentials) differs for different lattice parameters.

Another realistic strain condition can be induced by hydrostatic pressure, where the stress components along three directions are the same ($\sigma_{xx} = \sigma_{yy} = \sigma_{zz}$). The in-$c$-plane strain and out-of-c-plane strain now have the same sign, but
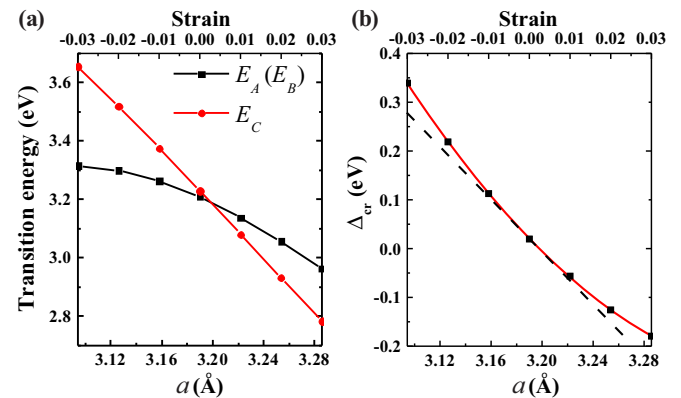

FIG. 3. (Color online) (a) Transition energies E_A ($=E_B$) and E_C of GaN under biaxial stress. (b) Crystal-field splitting of GaN under biaxial stress calculated with the HSE approach. Symbols correspond to calculated values, and solid lines represent second-order polynomial fits. The dashed line is a linear fit around the equilibrium lattice parameter.
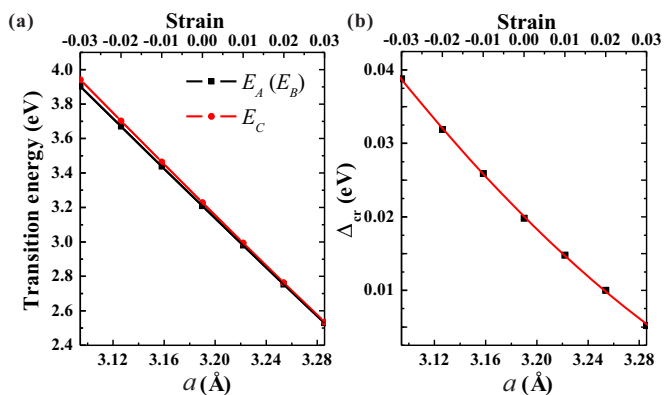
FIG. 4. (Color online) (a) Transition energies E_A (=E_B) and E_C of GaN under hydrostatic pressure. (b) Crystal-field splitting of GaN under hydrostatic pressure. The data are calculated using DFT and the HSE hybrid functional. Data points correspond to calculated values, and solid lines represent second-order polynomial fits. The dashed line is a linear fit around the equilibrium lattice parameter.

these strain components are not isotropic:

$$\varepsilon_{zz} = \frac{C_{11} + C_{12} - 2C_{13}}{C_{33} - C_{13}} \varepsilon_{xx},$$

$$\varepsilon_{xx} = \varepsilon_{yy} = \frac{C_{33} - C_{13}}{C_{33}(C_{11} + C_{12}) - 2C_{13}^2} \sigma_{zz}. \tag{10}$$

Under hydrostatic pressure, as shown in Fig. 4, both the transition energies and the crystal-field splitting change almost linearly in the strain range $\pm 3\%$.

C. Results for deformation potentials

We have seen that the dependence of the band energies on strain in general is nonlinear. However, over a small range of strains around a given lattice parameter, the variation can be regarded as linear. It is therefore still possible to define a single set of deformation potentials, choosing the experimental lattice parameters as the point of reference. By constraining the strain range to realistic strain conditions in the linear regime around the experimental lattice parameters, we derive a consistent and complete set of deformation potentials for all three nitrides. The resulting values are listed in Table III. The recommended values are those obtained with DFT-HSE, with the mixing parameter α adjusted to obtain a band gap that matches experiment. For comparison, for GaN and AlN, we also list results obtained with other exchange-correlation functionals and with HSE using the standard ($\alpha = 0.25$) mixing parameter. For InN, LDA and GGA results are not available since these functionals produce a negative band gap.

Table III shows that the calculated deformation potentials are sensitive to the choice of exchange-correlation functional. LDA and GGA-PBE data agree well with each other, but both of them show appreciable deviations from HSE results. The band-gap-related deformation potentials $a_{cz} - D_1$ and $a_{ct} - D_2$ obtained by HSE calculations are considerably larger in magnitude than those from LDA and GGA-PBE results. The HSE calculations with modified mixing parameters, which yield both very good structural properties and band structures,

are expected to also provide a reliable description of the change of band gaps under strain. The deformation potentials D_3, D_4, D_5, and D_6, which relate to the splitting of valence bands, are less sensitive to the choice of exchange-correlation functional. With the exception of $a_{cz} - D_1$, the deformation potentials decrease in absolute value from AlN to GaN to InN.

D. Deformation potentials: Validity, reliability, and comparison with experiment

We checked the validity of the HSE hybrid functional results by performing quasiparticle G_0W_0 calculations based on OEPx [44]. The comparison (included in Table III) shows that the deformation potentials of GaN obtained with DFT-HSE calculations are in good agreement with those obtained from G_0W_0 calculations (within 0.5 eV). Among these deformation potentials, $a_{cz} - D_1$ and $a_{ct} - D_2$ are more sensitive to the gap and hence present the most important test. The agreement with G_0W_0 data for these two deformation potentials validates the reliability of the HSE method in determining deformation potentials of nitrides and oxides [55]. Although both HSE and G_0W_0 calculations properly address the band-gap problem, here we recommend HSE, since the HSE calculations can self-consistently provide accurate results for both structural properties and band structures. Table III also shows that results obtained from HSE with modified mixing parameters are generally very close (within 0.3 eV) to the HSE results obtained with the default mixing parameter (25%). For GaN and AlN, we recommend HSE data obtained with the modified mixing parameters, since this approach provides more accurate atomic and electronic structures. Table III also lists the range of experimental data for deformation potentials of GaN, as reported in Ref. [52]; we note that our HSE results all fall within this (very wide) range.

Our deformation potential data also allow us to assess the accuracy of the quasicubic approximation. This approximation assumes a correlation of the physical properties of the wurtzite structure with those of the zinc-blende structure along the $\langle 111 \rangle$ direction due to the similarity of the local atomic bonding environment between wurtzite and zinc-blende structures. In the quasicubic approximation, the deformation potentials are related as follows: $D_3 = -2D_4$, $D_1 + D_3 = D_2$, and $D_3 + 4D_5 = \sqrt{2}D_6$. As a test, we checked the value of $D_3 + 2D_4$ (which should be zero in the quasicubic approximation), finding 1.43 eV for AlN, -0.52 for GaN, and -0.88 eV for InN. Clearly, neglecting the anisotropy of the wurtzite phase by applying the quasicubic approximation introduces significant inaccuracies in the determination of deformation potentials.

In Table III we also list the deformation potentials suggested for GaN by Vurgaftman and Meyer [52], which are obtained by averaging available data. Our HSE calculations for GaN yield systematically smaller absolute values than the Vurgaftman and Meyer numbers, with the exception of $a_{cz} - D_1$. For InN, Vurgaftman and Meyer recommended using the same deformation potentials as for GaN due to the lack of data. Our HSE values show that the deformation potentials of InN are much smaller than those of GaN, with differences in magnitude as large as several eV; use of the GaN values would therefore lead to significant errors.

TABLE III. Deformation potentials (eV) of wurtzite AlN, GaN, and InN obtained from DFT with LDA, GGA, and HSE functionals, and from the G_0W_0 quasiparticle approach. The calculated quantities are obtained at the experimental equilibrium lattice parameters. For GaN, the range of experimentally determined deformation potentials and the values recommended by Vurgaftman and Meyer (Ref. [52]) are also listed.

	Method	$a_{cz} - D_1$	$a_{ct} - D_2$	D_3	D_4	D_5	D_6
AlN	LDA	−3.44	−11.39	8.97	−3.95	−3.36	
	GGA	−3.39	−11.38	9.12	−4.01	−3.37	
	HSE ($\alpha = 0.25$)	−4.21	−12.07	9.22	−3.74	−3.30	−4.49
	HSE ($\alpha = 0.34$) (recommended)	−4.36	−12.35	9.17	−3.72	−2.93	−4.58
GaN	LDA	−4.56	−8.03	5.61	−3.03	−2.94	
	GGA	−4.46	−8.08	5.83	−2.98	−3.13	
	HSE ($\alpha = 0.25$)	−6.02	−8.98	5.45	−2.97	−2.87	−3.95
	HSE ($\alpha = 0.30$) (recommended)	−6.07	−8.88	5.38	−2.69	−2.56	−3.88
	G_0W_0@OEPx	−5.49	−8.84	5.80	−3.10		
	Expt. range	−9.6 ··· −3.1	−11.8 ··· −8.1	1.4 ··· 8.2	−4.1 ··· −0.7	−4.7 ··· −2.4	
	Vurgaftman and Meyer[a]	−4.90	−11.30	8.20	−4.10	−4.60	
InN	HSE ($\alpha = 0.25$) (recommended)	−3.64	−4.58	2.68	−1.78	−2.07	−3.02

[a]Reference [52].

E. Nonlinear effects on transition energies

To quantify the nonlinearities in the effect of strain on transition energies, we introduce a set of bowing parameters, b_1 to b_4. Assuming that the bowing parameters for the strain components along the x and y directions are equal to each other, the dependence of the transition energies ($E_{A/B}$ and E_C) on strain can be expressed as

$$
\begin{aligned}
E_{A/B} = {} & E_{A/B}(0) + (a_{cz} - D_1)\varepsilon_{zz} + (a_{ct} - D_2)\varepsilon_\perp \\
& - (D_3\varepsilon_{zz} + D_4\varepsilon_\perp) + (b_1 + b_3)\varepsilon_{zz}^2 + (b_2 + b_4)\varepsilon_\perp^2, \\
E_C = {} & E_C(0) + (a_{cz} - D_1)\varepsilon_{zz} + (a_{ct} - D_2)\varepsilon_\perp \\
& + b_1\varepsilon_{zz}^2 + b_2\varepsilon_\perp^2.
\end{aligned}
\tag{11}
$$

$E_{A/B}(0)$ and $E_C(0)$ denote the transition energies at experimental equilibrium lattice parameters, while $E_{A/B}$ and E_C are the transition energies when strain is applied. We obtain the bowing parameters for GaN by performing a quadratic fit of our transition-energy-strain data shown in Figs. 3 and 4. Similar calculations were performed for AlN and InN, and the resulting bowing parameters are listed in Table IV. This set of bowing parameters is an essential input to model the optical transitions in highly strained nitride heterostructures.

TABLE IV. Bowing parameters (eV) for strain effects on transition energies of wurtzite AlN, GaN, and InN obtained from DFT-HSE calculations. These bowing parameters should be used in conjunction with the recommended deformation potentials given in Table III. All quantities are obtained at the experimental equilibrium lattice parameters.

	b_1	b_2	b_3	b_4
AlN	−35.21	7.76	26.96	−14.50
GaN	−7.02	−0.63	−6.49	−7.66
InN	6.66	−1.51	−13.34	−4.94

IV. STRAIN EFFECTS IN InGaN ALLOYS

Now that we have a complete set of deformation potentials for GaN and InN, we can study the effects of strain on the band structure of In$_x$Ga$_{1-x}$N alloys. In$_x$Ga$_{1-x}$N layers grown pseudomorphically on GaN are under large biaxial stress due to the lattice mismatch. The resulting strain strongly affects the band structure. In addition, for c-plane-grown devices, the strain causes piezoelectric polarization, which induces electron-hole separation and lowers the radiative recombination rate and hence the efficiency. For this reason, growth in nonpolar and semipolar orientations, which avoid the polarization fields, has been pursued to improve the device efficiencies [8,9,56]. In such nonpolar and semipolar In$_x$Ga$_{1-x}$N layers, strain plays a crucial role in determining the polarization character of the emitted light. In this section, we explore the effects of strain on In$_x$Ga$_{1-x}$N alloys in detail.

A. Band gap of c-plane InGaN alloys

The incorporation of In into GaN lowers the band gap and allows the emission wavelength of In$_x$Ga$_{1-x}$N-based devices to be tuned over a wide spectral range from red to blue [58]. In$_x$Ga$_{1-x}$N epilayers grown on GaN are pseudomorphically strained, which affects the band gap. In addition, even in the absence of strain, the band-gap variation with In concentration is nonlinear, an effect known as band-gap bowing. For In$_x$Ga$_{1-x}$N, a surprisingly wide range of bowing parameters has been reported in the literature [17–19,57,59,60]. Moreover, the bowing parameter was found to depend on the In composition [57,59,61]. Here we aim to obtain a more accurate value for the bowing parameter by using our calculated deformation potentials to determine the effects of strain on the gap. These effects need to be subtracted from the experimental band-gap data before the effect of bowing can be determined.

It has been verified using hybrid functional calculations that the equilibrium lattice parameters of the In$_x$Ga$_{1-x}$N alloy can be obtained by linear interpolation between GaN and InN: $a_{\text{InGaN}} = a_{\text{InN}} \times x + a_{\text{GaN}} \times (1-x)$ (Ref. [61]). Similarly, the elastic constants and deformation potentials of the alloy systems can be determined from those of the pure nitrides
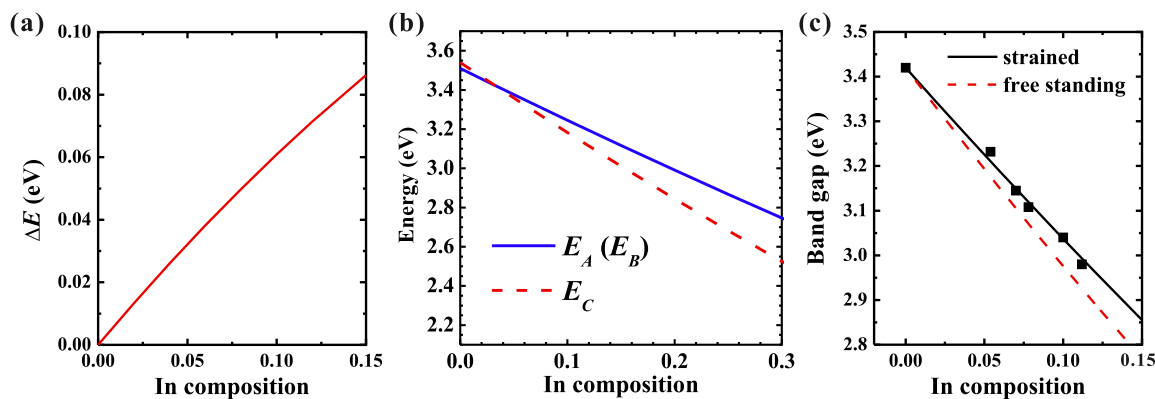
FIG. 5. (Color online) (a) Calculated band-gap change purely due to strain effects in an $In_xGa_{1-x}N$ alloy grown pseudomorphically on c-plane GaN. (b) Calculated transition energies of InGaN alloys grown on GaN as a function of In composition. (c) Band gap of $In_xGa_{1-x}N$ alloys with (solid line) and without (dashed line) strain effects. The bowing parameter is adjusted to provide an optimal fit to the experimental data of Refs. [17] and [57] (shown as black dots), resulting in a value $b = 2.0$ eV.

by linear interpolation: $C^{InGaN} = C^{InN} \times x + C^{GaN} \times (1 - x)$ and $D^{InGaN} = D^{InN} \times x + D^{GaN} \times (1 - x)$. For these physical quantities, treating the dependence on alloy composition up to linear order is sufficient. Any nonlinearities would have negligible effects on the relevant observables. The band gap of a free-standing alloy is calculated using the following equation: $E_g = E_{InN} \times x + E_{GaN} \times (1 - x) + b \times x(1 - x)$, with the bowing parameter b.

Assuming that the $In_xGa_{1-x}N$ epilayer is pseudomorphically strained to match the in-plane lattice constant of GaN, the in-c-plane biaxial strain components are determined by the lattice mismatch between InGaN and GaN: $\varepsilon_{xx} = \varepsilon_{yy} = (a_{GaN} - a_{InGaN})/a_{InGaN}$. The corresponding out-of-plane strain component is related to the in-plane strain by a combination of elastic constants of the alloy: $\varepsilon_{zz} = -\frac{2C_{13}}{C_{33}}\varepsilon_{xx}$. In the following, we use the elastic constants calculated by Wright *et al.* [54]. We use Eq. (2) to calculate the strain effects on the band gap of an InGaN alloy as a function of In composition. In previous work [17,57,59], strain effects on the band gap were assumed to be a linear function of the In fraction x. However, as shown in Fig. 5(a), such a linear relation does not hold true. The nonlinearity arises because the deformation potentials of InGaN alloys are not constant, i.e., they cannot be taken to be equal to those of GaN, but they depend on the In composition. Since the difference in deformation potentials between GaN and InN is quite large, the changes in band positions, which are products of deformation potentials and strains, exhibit distinct nonlinearities.

Using this more accurate treatment of strain effects, we can now rederive the bowing parameter of unstrained $In_xGa_{1-x}N$ alloys by fitting the experimental data of band gaps measured by McCluskey *et al.* [17,57]. As shown in Fig. 5(b), from our calculations, the three transition energies of the c-plane InGaN system decrease with increasing In composition, while the energy separation between HH/LH bands and the CH band increases with increasing In composition. The band gap of an $In_xGa_{1-x}N$ alloy as a function of In composition is shown in Fig. 5(c), for both a free-standing (unstrained) alloy and an alloy strained due to pseudomorphic growth on GaN. By fitting our calculated band gap (solid curve) to the experimental data [solid dots in Fig. 5(c)], a bowing parameter of 2.0 eV

is derived for $In_xGa_{1-x}N$ alloys within the composition range $0 < x < 0.1$. Strictly speaking, the bowing parameter depends on alloy composition, but the experimental data set is obviously not rich enough to address this additional complication, and the use of a fixed bowing parameter over this relatively narrow composition range is justified. The value $b = 2.0$ eV is smaller than the result derived by McCluskey *et al.* [57], but it agrees very well with the result obtained by recent first-principles hybrid functional calculations [61,62].

B. Strain effects on the polarization character of nonpolar *m*-plane InGaN

Nonpolar InGaN/GaN QWs have been proposed and fabricated as promising candidates for high-efficiency light emitters [8,63,64] because polarization fields in such devices are expected to be greatly reduced, resulting in enhanced efficiency. The lack of polarization fields, in turn, allows the use of wider QWs, which reduce the carrier density in the active layer for a given amount of injected current. These lower carrier densities are beneficial because they reduce losses due to Auger recombination, a loss mechanism that scales as the third power of the carrier density [6,65].

Light emitted from nonpolar InGaN/GaN QWs has been found to be polarized [9,14,56,66,67]. The emitted light has a preferential polarization along the $[11\bar{2}0]$ (x) direction, while the weaker transition has a polarization along the $[0001]$ (z) direction (i.e., along the c axis, which lies in the plane of the active layer in these nonpolar devices). Defining the polarization ratio as $\rho = (I_x - I_z)/(I_x + I_z)$, Masui *et al.* [14] further found that the polarization ratio increases with increasing In composition, and correspondingly the energy separation between the valence bands with x character and z character increases. Here we explore how strain affects the band ordering and polarization characteristics of the optical transition in such m-plane-oriented $In_xGa_{1-x}N$ alloys.

For $In_xGa_{1-x}N$ alloys grown on m-plane GaN substrates, the two principal directions in the m plane are $[11\bar{2}0]$ (x) and $[0001]$ (z), while the direction normal to the m plane is $[1\bar{1}00]$ (y). The in-m-plane strain components are determined by the lattice mismatch between the InGaN alloy and the GaN
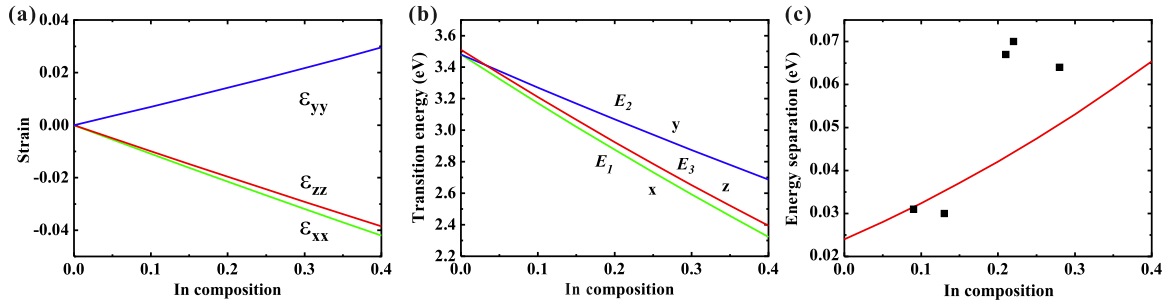
FIG. 6. (Color online) (a) Strain components in $In_xGa_{1-x}N$ alloys grown pseudomorphically on m-plane GaN. (b) Transition energies of m-plane $In_xGa_{1-x}N$ alloys. (c) Energy separation between the topmost two valence bands (E_1 and E_3). Experimental data from Masui *et al.* [14] are shown as black dots.

substrate, while the out-of-plane strain component (along the y direction) is determined by the relation $\varepsilon_{yy} = -\frac{C_{11}}{C_{33}}\varepsilon_{xx} - \frac{C_{12}}{C_{33}}\varepsilon_{zz}$. Assuming that the InGaN film is perfectly strained by the underlying GaN without any strain relaxation, the strain components in the alloy are calculated from the lattice mismatch and elastic constants, as shown in Fig. 6(a). The strain component along the x direction ε_{xx} is compressive, while that along the y direction ε_{yy} is tensile. This difference between ε_{xx} and ε_{yy} (which is absent in $In_xGa_{1-x}N$ alloys grown along the polar c direction) plays a crucial role in the modification of the band structure of m-plane $In_xGa_{1-x}N$ alloys by splitting the HH and LH bands and leading to polarized light emission.

With our deformation potentials and the expressions for band energies in Eq. (4), we calculate the transition energies of an $In_xGa_{1-x}N$ alloy as a function of In composition, as shown in Fig. 6(b). The difference between ε_{xx} and ε_{yy} lowers the symmetry of the wurtzite system from C_{6v} to C_{2v} and splits the HH and LH bands. These two bands are denoted now as E_1 and E_2, respectively, since the strain perturbation breaks the original two $|X \pm iY\rangle$ states into p_x-like and p_y-like states. By solving the strained $\mathbf{k \cdot p}$ Hamiltonian, we find that the eigenstate of the E_1 band has p_x character while that of the E_2 band has p_z character. Furthermore, at a very low In composition ($x = 0.04$), the E_2 valence band crosses the CH band, which is p_z-like and denoted as the E_3 band. This indicates that in m-plane $In_xGa_{1-x}N$ alloys with In compositions higher than 4%, the band ordering near the valence-band edge is E_1, E_3, and E_2 in order of decreasing electron energy. The dominant optical transition is therefore from the conduction band to the E_1 band, and the emitted light from this transition has polarization mainly along the x direction. The next possible but much weaker transition is from the CBM to the E_3 band, leading to polarization along the z direction. Such a band ordering and polarization character of the emitted light is consistent with recent experimental observations [9,14,67].

As shown in Fig. 6(c), the energy separation between the E_1 and E_3 valence bands increases with increasing In composition. This implies that the relative hole occupation of the lower band decreases and the polarization ratio increases, in agreement with the experimental observations of Ref. [14] at low In compositions. A discontinuous change in the experimental data occurs around an In composition of 0.2. This variation cannot be explained if we assume that the

alloy is perfect and fully strained by the underlying GaN. The discrepancy is possibly due to In segregation, or to strain relaxation in these nonpolar $In_xGa_{1-x}N$ alloys with high In fraction.

C. The role of strain in the valence-band structure of semipolar InGaN alloys

Semipolar QW orientations have been proposed to increase the efficiency of light emitters. In these orientations, the effect of spontaneous and piezoelectric polarization fields is reduced and thereby the carrier overlap is increased [8,11,63,64]. Similar to the nonpolar case, growth of InGaN on GaN along semipolar directions leads to strain conditions different from those in conventional growth along the c direction. Strain in semipolar InGaN grown on GaN is characterized by the shear strain and anisotropic strain in the c plane. This affects the splitting of the uppermost valence bands and hence the polarization of the emitted light. Optical anisotropy has been observed for semipolar devices [11,12,45,68,69]. In addition, in semipolar ($11\bar{2}2$) InGaN QWs grown on GaN, the dominant polarization direction was found to switch from [$1\bar{1}00$] (perpendicular to the c axis) to [$\bar{1}\bar{1}23$] when the In concentration was increased above 30% [70,71].

Three factors critically influence the band structure of InGaN QWs and therefore the polarization of the emitted light: indium concentration, strain, and quantum confinement. Based on $\mathbf{k \cdot p}$ modeling, Yamaguchi predicted that the QW thickness strongly affects the polarization [72]. This seems qualitatively consistent with the results of Masui *et al.*, who observed an enhancement in optical polarization for thinner QWs [71]. However, in Yamaguchi's work, the magnitude of this quantum confinement effect is very sensitive to the choice of Luttinger parameters [51] and can range from 2 to 20 meV for 2-nm-thick QWs. Ueda *et al.*, on the other hand, found no appreciable QW thickness effect [70]. They proposed strain to be the dominant factor, and they derived a large shear-strain deformation potential of $D_6 = -8.8$ eV from their measurements [70]. Our own study of quantum confinement [73] also produced very small differences compared to bulk calculations; the main cause of polarization switching must therefore be the strain.

In previous work [21], we found that anisotropic strain (through the deformation potential D_5) and shear strain (through the deformation potential D_6) have opposite effects

on the valence-band separation. A switch in the band ordering may occur if the shear strain and/or the deformation potential D_6 are large enough. However, using our consistent set of deformation potentials, we found no evidence of any switch in band ordering with increasing In concentration [21]. Note that the D_6 value derived by Ueda *et al.* [70] is much larger than any of our calculated values. We conclude that the underlying cause of the polarization switching remains unresolved. One possible explanation is that the switching is due to inhomogeneities of In concentrations and strain distributions in InGaN alloys with high In content. A recent theoretical work supports our conclusion that the polarization switching with increasing carrier density may be attributed to inhomogeneous strain distribution in the InGaN quantum wells [74].

Polarized light emission has also been observed in semipolar InGaN QWs grown in (20$\bar{2}$1), (30$\bar{3}$1), and (30$\bar{3}\bar{1}$) orientations, and in all cases our calculated deformation potentials have provided results for polarization ratios in good agreement with the experimental observations [11,12], providing further confidence in the accuracy of our values.

V. CONCLUSION

We have studied strain effects on the band structure of wurtzite AlN, GaN, and InN using a first-principles approach based on density functional theory with a hybrid functional. We observed nonlinearities in the strain dependence and obtained a set of strain bowing parameters that can be used to account for nonlinear effects on band structure in highly strained nitrides. For the linear regime around the experimental lattice parameters, we have presented a complete and consistent set of deformation potentials for the three nitride materials. Examples of how our deformation potentials can be used in the interpretation of experimental data on InGaN alloys and quantum wells were provided. Together with the Luttinger band parameters [51], the deformation potentials constitute essential input for device modeling, and they will allow accurate predictions of band positions under realistic strain conditions.

[1] T. M. S. Nakamura and M. Senoh, Jpn. J. Appl. Phys. **30**, L1998 (1991).

[2] S. Nakamura, M. Senoh, S. Nagahama, N. Iwasa, T. Yamada, T. Matsushita, Y. Sugimoto, and H. Kiyoku, Appl. Phys. Lett. **69**, 4056 (1996).

[3] U. K. Mishra, P. Parikh, and Y. F. Wu, Proc. IEEE **90**, 1022 (2002).

[4] Y. C. Shen, G. O. Mueller, S. Watanabe, N. F. Gardner, A. Munkholm, and M. R. Krames, Appl. Phys. Lett. **91**, 141101 (2007).

[5] A. David and N. F. Gardner, Appl. Phys. Lett. **97**, 193508 (2010).

[6] E. Kioupakis, P. Rinke, K. T. Delaney, and C. G. Van de Walle, Appl. Phys. Lett. **98**, 161107 (2011).

[7] A. E. Romanov, T. J. Baker, S. Nakamura, and J. S. Speck, J. Appl. Phys. **100**, 023522 (2006).

[8] B. A. Haskell, F. Wu, S. Matsuda, M. D. Craven, P. T. Fini, S. P. DenBaars, J. S. Speck, and S. Nakamura, Appl. Phys. Lett. **83**, 1554 (2003).

[9] T. Koyama, T. Onuma, H. Masui, A. Chakraborty, B. A. Haskell, S. Keller, U. K. Mishra, J. S. Speck, S. Nakamura, S. P. DenBaars *et al.*, Appl. Phys. Lett. **89**, 091906 (2006).

[10] P. S. Hsu, K. M. Kelchner, A. Tyagi, R. M. Farrell, D. A. Haeger, K. Fujito, H. Ohta, S. P. DenBaars, J. S. Speck, and S. Nakamura, Appl. Phys. Express **3**, 052702 (2010).

[11] Y. Zhao, S. Tanaka, Q. Yan, C.-Y. Huang, R. B. Chung, C.-C. Pan, K. Fujito, D. Feezell, C. G. Van de Walle, J. S. Speck *et al.*, Appl. Phys. Lett. **99**, 051109 (2011).

[12] Y. Zhao, Q. Yan, D. Feezell, K. Fujito, C. G. Van de Walle, J. S. Speck, S. P. Den Baars, and S. Nakamura, Opt. Express **21**, A53 (2013).

[13] S. H. Park and S. L. Chuang, Phys. Rev. B **59**, 4725 (1999).

[14] H. Masui, H. Yamada, K. Iso, S. Nakamura, and S. P. Denbaars, J. Phys. D **41**, 225104 (2008).

[15] M. Azize and T. Palacios, J. Appl. Phys. **108**, 023707 (2010).

[16] C. E. Dreyer, A. Janotti, and C. G. Van de Walle, Appl. Phys. Lett. **102**, 142105 (2013).

[17] M. D. McCluskey, C. G. Van de Walle, L. T. Romano, B. S. Krusor, and N. M. Johnson, J. Appl. Phys. **93**, 4340 (2003).

[18] K. P. O'Donnell, R. W. Martin, C. Trager-Cowan, M. E. White, K. Esona, C. Deatcher, P. G. Middleton, K. Jacobs, W. V. der Stricht, C. Merlet *et al.*, Mater. Sci. Eng. B **82**, 194 (2001).

[19] C. A. Parker, J. C. Roberts, S. M. Bedair, M. J. Reed, S. X. Liu, N. A. El-Masry, and L. H. Robins, Appl. Phys. Lett. **75**, 2566 (1999).

[20] K. Kojima, H. Kamon, M. Funato, and Y. Kawakami, Phys. Status Solidi C **5**, 3038 (2008).

[21] Q. Yan, P. Rinke, M. Scheffler, and C. G. Van de Walle, Appl. Phys. Lett. **97**, 181102 (2010).

[22] W. Scheibenzuber, U. Schwarz, R. Veprek, B. Witzigmann, and A. Hangleiter, Phys. Status Solidi C **7**, 1925 (2010).

[23] M. Smith, G. D. Chen, J. Y. Lin, H. X. Jiang, M. A. Khan, C. J. Sun, Q. Chen, and J. W. Yang, J. Appl. Phys. **79**, 7001 (1996).

[24] G. D. Chen, M. Smith, J. Y. Lin, H. X. Jiang, S. H. Wei, M. A. Kahn, and C. J. Sun, Appl. Phys. Lett. **68**, 2784 (1996).

[25] B. Gil and A. Alemu, Phys. Rev. B **56**, 12446 (1997).

[26] W. Shan, R. J. Hauenstein, A. J. Fischer, J. J. Song, W. G. Perry, M. D. Bremser, R. F. Davis, and B. Goldenberg, Phys. Rev. B **54**, 13460 (1996).

[27] S. Chichibu, T. Azuhata, T. Sota, H. Amano, and I. Akasaki, Appl. Phys. Lett. **70**, 2085 (1997).

[28] B. Gil, M. Moret, O. Briot, S. Ruffenach, C. Giesen, M. Heuken, S. Rushworth, T. Leese, and M. Succii, J. Cryst. Growth **311**, 2798 (2009).

[29] G. L. Bir and G. E. Pikus, *Symmetry and Strain-Induced Effects in Semiconductors* (Wiley, New York, 1974).

[30] R. Ishii, A. Kaneta, M. Funato, Y. Kawakami, and A. A. Yamaguchi, Phys. Rev. B **81**, 155202 (2010).

[31] R. Ishii, A. Kaneta, M. Funato, and Y. Kawakami, Phys. Lett. B **87**, 235201 (2013).

[32] M. Suzuki and T. Uenoyama, J. Appl. Phys. **80**, 6868 (1996).

[33] S. L. Chuang and C. S. Chang, Phys. Rev. B **54**, 2491 (1996).

[34] S. Ghosh, P. Waltereit, O. Brandt, H. T. Grahn, and K. H. Ploog, Phys. Rev. B **65**, 075202 (2002).

[35] K. Shimada, T. Sota, and K. Suzuki, J. Appl. Phys. **84**, 4951 (1998).

[36] W. W. Chow, A. F. Wright, A. Girndt, F. Jahnke, and S. W. Koch, in *Symposium D – Gallium Nitride and Related Materials II*, edited by C. R. Abernathy, H. Amano, and J. C. Zolper, MRS Proceedings, 468 (MRS, Pittsburgh, 1997), pp. 468–487.

[37] J. A. Majewski, M. Städele, and P. Vogl, in *Symposium N – III-V Nitrides*, edited by F. A. Ponce, T. D. Moustakas, I. Akasaki, and B. A. Monemar, MRS Proceedings 449 (MRS, Pittsburgh, 1997), pp. 449–887.

[38] Q. Yan, P. Rinke, M. Scheffler, and C. G. Van de Walle, Appl. Phys. Lett. **95**, 121111 (2009).

[39] Q. Yan, P. Rinke, M. Winkelnkemper, A. Qteish, D. Bimberg, M. Scheffler, and C. G. Van de Walle, Semicond. Sci. Technol. **26**, 014037 (2011).

[40] A. A. Yamaguchi, Y. Mochizuki, C. Sasaoka, A. Kimura, M. Nido, and A. Usui, Appl. Phys. Lett. **71**, 374 (1997).

[41] P. Misra, U. Behn, O. Brandt, H. T. Grahn, B. Imer, S. Nakamura, S. P. Den Baars, and J. S. Speck, Appl. Phys. Lett. **88**, 161920 (2006).

[42] H. Y. Peng, M. D. McCluskey, Y. M. Gupta, M. Kneissl, and N. M. Johnson, Phys. Rev. B **71**, 115207 (2005).

[43] J. Heyd, G. E. Scuseria, and M. Ernzerhof, J. Chem. Phys. **124**, 219906 (2006).

[44] P. Rinke, A. Qteish, J. Neugebauer, C. Freysoldt, and M. Scheffler, New J. Phys. **7**, 126 (2005).

[45] H. Masui, T. J. Baker, M. Iza, H. Zhong, S. Nakamura, and S. P. DenBaars, J. Appl. Phys. **100**, 113109 (2006).

[46] G. B. Ren, Y. M. Liu, and P. Blood, Appl. Phys. Lett. **74**, 1117 (1999).

[47] L. Cláudio de Carvalho, A. Schleife, F. Fuchs, and F. Bechstedt, Appl. Phys. Lett. **97**, 232101 (2010).

[48] P. E. Blöchl, Phys. Rev. B **50**, 17953 (1994).

[49] G. Kresse and J. Furthmüller, Phys. Rev. B **54**, 11169 (1996).

[50] J. Heyd, G. E. Scuseria, and M. Ernzerhof, J. Chem. Phys. **118**, 8207 (2003).

[51] P. Rinke, M. Winkelnkemper, A. Qteish, D. Bimberg, J. Neugebauer, and M. Scheffler, Phys. Rev. B **77**, 075202 (2008).

[52] I. Vurgaftman and J. R. Meyer, J. Appl. Phys. **94**, 3675 (2003).

[53] V. Y. Davydov, A. A. Klochikhin, R. P. Seisyan, V. V. Emtsev, S. V. Ivanov, F. Bechstedt, J. Furthmüller, H. Harima, A. V. Mudryi, J. Aderhold *et al.*, Phys. Status Solidi B **229**, R3 (2002).

[54] A. F. Wright, J. Appl. Phys. **82**, 2833 (1997).

[55] Q. Yan, P. Rinke, M. Winkelnkemper, A. Qteish, D. Bimberg, M. Scheffler, and C. G. Van de Walle, Appl. Phys. Lett. **101**, 152105 (2012).

[56] N. F. Gardner, J. C. Kim, J. J. Wierer, Y. C. Shen, and M. R. Krames, Appl. Phys. Lett. **86**, 111101 (2005).

[57] M. D. McCluskey, C. G. Van de Walle, C. P. Master, L. T. Romano, and N. M. Johnson, Appl. Phys. Lett. **72**, 2725 (1998).

[58] M. Y. T. Mukai and S. Nakamura, Jpn. J. Appl. Phys. **38**, 3976 (1999).

[59] C. G. Van de Walle, M. McCluskey, C. P. Master, L. T. Romano, and N. M. Johnson, Mater. Sci. Eng. B **59**, 274 (1999).

[60] S. Pereira, M. R. Correia, T. Monteiro, E. Pereira, E. Alves, A. D. Sequeira, and N. Franco, Appl. Phys. Lett. **78**, 2137 (2001).

[61] P. G. Moses and C. G. Van de Walle, Appl. Phys. Lett. **96**, 021908 (2010).

[62] P. Moses, M. S. Miao, Q. Yan, and C. G. Van de Walle, J. Chem. Phys. **134**, 084703 (2011).

[63] K. Nishizuka, M. Funato, Y. Kawakami, S. Fujita, Y. Narukawa, and T. Mukai, Appl. Phys. Lett. **85**, 3122 (2004).

[64] A. Tyagi, Y.-D. Lin, D. A. Cohen, M. Saito, K. Fujito, J. S. Speck, S. P. DenBaars, and S. Nakamura, Appl. Phys. Express **1**, 091103 (2008).

[65] E. Kioupakis, Q. Yan, and C. G. Van de Walle, Appl. Phys. Lett. **101**, 231107 (2012).

[66] U. Behn, P. Misra, H. T. Grahn, B. Imer, S. Nakamura, S. P. DenBaars, and J. S. Speck, Phys. Status Solidi A **204**, 299 (2007).

[67] H. Tsujimura, S. Nakagawa, K. Okamoto, and H. Ohta, Jpn. J. Appl. Phys. **46**, L1010 (2007).

[68] M. Ueda, K. Kojima, M. Funato, Y. Kawakami, Y. Narukawa, and T. Mukai, Appl. Phys. Lett. **89**, 211907 (2006).

[69] K. Kojima, M. Funato, Y. Kawakami, S. Masui, S. Nagahama, and T. Mukai, Appl. Phys. Lett. **91**, 251107 (2007).

[70] M. Ueda, M. Funato, K. Kojima, Y. Kawakami, Y. Narukawa, and T. Mukai, Phys. Rev. B **78**, 233303 (2008).

[71] H. Masui, H. Asamizu, A. Tyagi, N. F. DeMille, S. Nakamura, and S. P. DenBaars, Appl. Phys. Express **2**, 071002 (2009).

[72] A. A. Yamaguchi, Phys. Status Solidi C **5**, 2329 (2008).

[73] C. Roberts, Q. Yan, M. S. Miao, and C. G. Van de Walle, J. Appl. Phys. **111**, 073113 (2012).

[74] S. H. Park, D. Mishra, Y. E. Pak, C. Y. Park, S. H. Yoo, Y. H. Cho, M. B. Shim, S. Hwang, and S. Kim, Appl. Phys. Lett. **103**, 201108 (2013).